

Torsional oscillations of the Earth's core

Raymond Hide^{1,2}, Dale H. Boggs¹, Jean O. Dickey¹

¹Jet Propulsion Laboratory, California Institute of Technology, 4800 Oak Grove Drive, Pasadena, CA 91109-8099, USA

²Physics Department (Atmospheric, Oceanic and Planetary Physics), Oxford University, Clarendon Laboratory, Parks Road, Oxford OX2 3PU, England, UK

Abstract. Torsional oscillations of the Earth's liquid metallic outer core are investigated by dividing the core into twenty imaginary equi-volume annuli coaxial with the axis of rotation of the Earth and determining temporal fluctuations in the axial component of angular momentum of each annulus under the assumption of iso-rotation on cylindrical surfaces. With the available velocity fields just below the core-mantle interface as derived from geomagnetic secular variation observations, it is possible to investigate core angular momentum (CAM) over fifteen decades from 1840–1990. This interval is much shorter than the expected periods of non-axisymmetric magnetohydrodynamic (MHD) oscillations of the core—one class of shear waves at sub-seismic frequencies— but it does exceed that of the expected period of axisymmetric MHD torsional oscillations. The dominant period seen in the data is about 65 years. If this can be interpreted as being that of the gravest mode of MHD torsional oscillation, then the implied value of B_p (the average strength of the non-axial component of the poloidal part of the geomagnetic field) is about $2 \times 10^{-4} T$ (2 gauss), roughly half the average strength of the (poloidal) geomagnetic field in the lower reaches of the mantle and very much less than the likely average strength of the toroidal magnetic field in the core, which may be as high as $10^{-2} T$ (10^2 gauss). CAM fluctuations are most pronounced in the mid-latitudes and are generally

out of phase with those occurring in equatorial regions. They are roughly in phase with decadal length-of-day (LOD) fluctuations, especially after about 1870, with the dominant variability period of -65 years. The largest positive correlations (0.8 when data before 1867.5 are excluded) are observed in the mid-latitudes with a maximum at zero lag and with secondary peaks at 67 yrs and at -64 years, again implying a -65 year mode. Propagation of CAM anomalies from the equatorial to polar regions is evident in both the time-latitude dependence of CAM and its latitudinal correlation with length of day fluctuations.

Introduction

Motions in the Earth's liquid metallic outer core produce the main geomagnetic field by self-exciting magnetohydrodynamic dynamo action (I). Driven by buoyancy forces due to the action of density inhomogeneities associated with differential heating and cooling, core motions are strongly influenced not only by Coriolis forces due to the Earth's rotation and the geometry of the bounding surfaces but also by Lorentz forces due to the presence of electric currents and magnetic fields within the core. The main aim of the present study is to shed further light on the dynamical processes within the Earth's deep interior that give rise to decadal fluctuations in the rate of rotation of the solid Earth, and involve angular momentum transfer not only between the core and the overlying mantle but also between different parts of the core.

Considerations of fluctuations in angular momentum within a fluid system and of the exchange of angular momentum between the fluid system and the regions with which it is in contact are of fundamental importance in realistic dynamical studies, as exemplified by investigations of planetary-scale motions in atmospheres and oceans (2-6). Strong indirect evidence of angular momentum exchange between the core and the overlying mantle stems from general quantitative considerations made in the first realistic attempts to interpret determinations of length of day (LOD) fluctuations on decadal time

scales, for the LOD is an inverse measure of angular momentum of the solid Earth (M_S). Indeed, it has long been generally accepted that irregular LOD fluctuations on such time scales must be due largely to core motions (see e.g. (7, 8)).

It is because of the high density of the core, more than 10^4 times that of the atmosphere, that these two fluid regions of the Earth (the core and atmosphere) are able to produce effects on the rotation of the solid Earth that are generally comparable in magnitude. The amplitude of seasonal atmospheric variations, for example, are about a millisecond (ms), while decadal fluctuations can be as large as 5 ms. The core acts on longer time scales than the atmosphere, for the speed of core motions is typically 10^{-4} times that of atmospheric winds; one week for the atmosphere thus translates into about a century for the core, so the 150 years of geomagnetic data available for the present study can provide no more than a glimpse of what might be happening in the core. In contrast, work on the interpretation of fluctuations in the Earth's rotation on shorter sub-decadal timescales in terms of dynamical processes in the atmosphere (and ocean) (2–6) is more advanced owing, in large part, to the abundant meteorological data, which are well-sampled in time and relatively well-sampled in space. The characteristic periods of the relevant phenomena studied are generally much shorter than the data span, and data analyses are correspondingly robust. It is possible to investigate angular momentum transfer between different parts of the atmosphere, thereby elucidating processes of central importance in theories of the general circulation of the atmosphere and its interaction with the underlying planet. It is unlikely that detailed magnetic observations from much earlier times can be obtained from existing records, so the best use has to be made of the data sets currently available.

Angular momentum budget

Denote by M_S the axial component of the angular momentum of the solid Earth and by M'' that of the liquid core. On decadal time scales the equation

$$\frac{dM_s}{dt} = - \frac{dM}{dt} \quad (1)$$

expresses angular momentum conservation to better than 10% (the residual being largely associated with atmospheric and oceanic effects). M is given by the axial component of

$$\iiint \rho(\mathbf{r}, t) \mathbf{r} \times [\boldsymbol{\Omega} \times \mathbf{r} + \mathbf{u}] d\tau \quad (2)$$

where $\rho(\mathbf{r}, t)$ is the mass density at a general point P in a frame of reference with its origin at the Earth's center of mass and which rotates with the mantle with angular velocity $\boldsymbol{\Omega}$ relative to an inertial frame and \mathbf{u} is the Eulerian relative flow velocity, and $d\tau$ is an element of volume of the liquid core, over the whole of which the volume integral is taken.

Thus, to conserve the angular momentum of the whole system, any fluctuations in the total angular momentum of the liquid outer core must be accompanied by fluctuations in the angular momentum not only of the overlying solid mantle but also of the underlying solid inner core which, being a good electrical conductor, should be tightly coupled by Lorentz forces to the liquid core. However, in comparison with the liquid core, the volume of the solid inner core is small, no more than that of one of the twenty equi-volume annuli into which we divide the core in the present study (see Figure 1). The moment of inertia of the solid inner core is even smaller in comparison, much less than 1% of that of the outer core. Given the accuracy level of angular momentum budget analyses, any contributions to dM_s/dt associated with possible fluctuations in the motion of the inner core can be neglected. Further justification for this assumption arises from new seismological studies (9, 10) of the relative rotation of the inner core, as well as from related studies stimulated by this important new development in core dynamics (11–13).

The LOD data used here are a self-consistent time-series resulting from the analysis of lunar occultations prior to 1955.5. after which a combination of astronomical and modern geodetic techniques are utilized (14). There is evidence based on solar eclipses and other data (15) that over the past 2700 years the LOD has increased at an average rate of at 1.70 ± 0.05 ms/cy. This can be attributed to two main agencies, namely tidal braking of the Earth's spin (2.3 ± 0.1 ms/cy) and changes in the Earth's polar moment of inertia associated with "post-glacial rebound" (-0.6 ± 0.1 ms/cy). This trend of 1.7 ms/cy was removed from the LOD series before comparing it with core angular momentum $M(t)$; results were shown to be insensitive to this trend. The residual found when the trend revealed by eclipse observations has been removed from the LOD time series shows some evidence of slow fluctuations, the detailed spectrum of which cannot yet be determined owing to errors and sparsity in the data. At about 4 ms, the semi-amplitude of these long-period variations is roughly the same as that of the LOD fluctuations on much shorter decadal time scales as deduced from observatory data obtained over the past century or so. These findings imply that core motions may excite a fairly flat spectrum of LOD fluctuations over time scales ranging from decades to centuries and longer.

Determinations of core angular momentum

Just as it is convenient to divide the atmosphere into the troposphere, stratosphere and higher regions, and the oceans into the thermocline and lower regions, the liquid metallic core can be divided into the "torosphere," where the toroidal magnetic field is so strong that Lorentz forces are comparable in magnitude with Coriolis forces (16), and the overlying "polosphere" where the toroidal magnetic field is typically no stronger than the poloidal field, Lorentz forces being correspondingly much weaker than Coriolis forces (17). Owing to the presence of the solid inner core, Coriolis forces inhibit flow across the imaginary cylindrical surface that is tangential to the inner core at the equator and

intersects the outer core at latitudes $\pm 66^\circ$ (see Figure 1). So it is convenient to sub-divide the liquid core further into “polar” regions lying within the tangent cylinder and “extrapolar” regions lying outside the cylinder. This scheme proves useful not only in work on the dynamics of the Earth’s core (11, 18) but also in studies of other geophysical and astrophysical fluids, such as the various fluid layers of Jupiter and Saturn and the convective outer layers of the Sun. Some justification for the scheme is provided by the laboratory experiments on thermal convection in an electrically-insulating rotating fluid upon which the scheme was originally based (19), and further justification comes from the flow fields produced in numerical models of buoyancy-driven MHD flows in the Earth’s core (12, 13). In both cases motions are more vigorous in extrapolar regions, particularly in mid-latitudes, than they are in the comparatively quiescent polar regions.

For the purpose of the present paper, we suppose here that the Earth’s liquid metallic outer core is bounded by concentric spherical surfaces of radii $c = 3480$ km and $b = 1222$ km (see Figure 1) and we divide the core into $Q = 20$ cylindrical annuli of equal volume (20). The total axial angular momentum $\mu_q(t; Q)$ associated with relative core motions with Eulerian flow velocity $\mathbf{u}(\mathbf{r}, t) = (u, v, w)$ at a general point P with spherical polar coordinates (r, θ, ϕ) is given by

$$\mu_q(t; Q) \equiv \frac{4\pi}{3Q} (c^3 - b^3) \{\rho w r \sin \theta\}_q. \quad (3)$$

Here $\rho = \rho(r, \theta, \phi, t)$ is the density at P , $w = w(r, \theta, \phi, t)$ and the symbol $\{\}$ denotes the spatial average over the volume occupied by the q -th annulus (see Figure 1). One of the main objectives of the present study is to determine temporal fluctuations in $\mu_q(t; Q)$ for all q using available data and to examine (the fluctuations for evidence of torsional oscillations.

Owing to the inaccessibility of the core, direct determinations of $\mathbf{u}(\mathbf{r}, t)$ and $\rho(\mathbf{r}, t)$ are impossible. But methods have now been developed for making indirect

estimates of the (θ, ϕ) components (v_s, w_s) of u_s , the Eulerian flow velocity just below the CMB, where $r \doteq c$, from geomagnetic secular variation data under various geophysically plausible assumptions (21). The data used in the present study cover the interval from 1840 to 1990 and were kindly provided by Dr. Andrew Jackson. By introducing the additional assumption that variations in ρw in the direction parallel to the rotation axis are negligibly small (see e.g. (18, 22, 23)), ρw can be replaced in Eq. (2) by the known quantity

$$\frac{1}{2} \bar{\rho} [w_s(\theta, \phi, t) + w_s(\pi - \theta, \phi, t)]. \quad (4)$$

This gives for $\mu_q(t; Q)$ the approximate relationship

$$\mu_q(t; Q) = \frac{2\pi\rho_s c(c^3 - b^3)}{3Q} \langle [w_s(\theta, \phi, t) + w_s(\pi - \theta, \phi, t)] \sin \theta \rangle_q \quad (5)$$

over the surface area of the q -th annulus, covering the ranges $0 \leq \phi \leq 2\pi$ and $\theta_{q-1} \leq \theta \leq \theta_q$ (see 20), where $\langle \rangle_q$ signifies the spatial average. Though difficult to justify rigorously on theoretical grounds, the additional assumption of isorotation on co-axial cylindrical surfaces has been discussed and used with remarkable success in important recent studies by Jault and LeMouél and others of the angular momentum budget of the core-mantle system (22, 23). Combining Eq. (5) and (2) gives

$$M(t) = \sum_{q=1}^Q \mu_q(t; Q), \quad (6)$$

as a rough measure of the total axial angular momentum associated with relative motions in the cm-c (cf. Eq. (1) and (22)).

Results and discussion

The total core angular momentum $M(t)$ as well as the contributions from the individual cylinders $\mu_q(t; 20)$ are displayed in Fig. 2(a). Here we introduce the “equivalent millisecond unit” (emsu), defined as that amount of axial angular momentum, namely $0.60 \times 10^{26} \text{ kg m}^2 \text{ s}^{-1}$, which, if transferred to the overlying solid Earth would, if the solid Earth were perfectly rigid, reduce the length of the day (LOD) by 1 ms. Two broad maxima occur in $M(t)$ with the highest value attained around 1900 with “full width half max” (FWHM) of -25 years (Fig. 2a). The second smaller maximum has its peak near 1970 with FWHM of 15 years. There is considerable range of variability of the individual bands [Fig. 2(b)] with time-averaged total CAM $\bar{M}(t)$ (say) being negative (-0.237 emsu). The equatorial band ($q = 20$) with the largest lever arm produces the largest contribution with time-averaged values being largely negative (i.e. $\mu_q(t; 20) \approx -0.4$ esu). The two large peaks are clearly seen in the equatorial annuli (Fig. 2a); with the first peak near 1885 corresponding to the plateau region near 1885 in the total CAM and the second peak occurring near the 1975 maximum in total CAM. The other bands are highly bimodal as well, with cylinders 16–19 having their maxima near 1885 and 1950, while cylinders 3–15 have maxima near 1910 and 1970. The contribution from bands 1–3 with a short lever arm are small with the largest contribution near 1910.

The three dimensional diagram (Fig. 3) of the contributions from the individual cylinders (M_i) given as a function of time permits unique insight into core dynamics. The dominant feature is a strong -65 year oscillation that is particularly evident in the midlatitude bands (3–15). Note that the maxima in the midlatitude coincide in time with the largest geomagnetic jerks events over the time period considered, namely, 1912 and 1969 (24). Variability in cylinders 16–20 generally precedes that in the midlatitudes, with results suggestive of angular momentum propagation from the equatorial toward midlatitude region. On the basis of Figs. 1–3 and Table 1, we divide the core into three

regions: polar (P), midlatitude (ML) and equatorial (EQ). The polar region (where $q = 1, 2, 3$) is a natural division given the dimension of the solid inner core (Fig. 1), whereas the division into midlatitude ($q = 4-15$) and equatorial ($q = 16-20$) is motivated by the characteristic behavior of these two regions. The comparison of LOD fluctuations with total and regional $M(t)$ (Fig. 4) shows that the decadal LOD variability is well matched with $M(t)$, especially after 1870. Data prior to 1870 are not as robust as the more modern data, with a mismatch occurring during the series between 1840–1870. The maximum correlation between M and LOD (Table 1) is 0.58 at a lag of -17.5 yrs when the full series (1840-1990) is considered and is 0.64 with a lag of -5 yrs with the shorter series (1870-1990). The $M(t)$ data spacing is 2.5 yrs; hence, care must be taken in the interpretation of the lag of the latter correlation. The contribution from midlatitudes (\dot{M}_{ML}) (Fig. 3 and 4) dominates M and accounts for a major portion of the LOD decadal variability (56.9% for the full series and 74.9% for the short series). M_{ML} is in phase with LOD, having a maximum correlation of 0.8 with the shorter series and 0.5 for the full series (Fig. 5); secondary maxima occur at 67 and -64 years, consistent with the -65 year periodicity.

The equatorial CAM (M_{EQ} ; cylinders 16–20) time series is bimodal, with maxima at 1885 and 1950, and leads the M_{ML} by -20 years (Fig. 4). The correlation of M_{EQ} with LOD has a principal maximum at a lead of -25 years with secondary maxima near 44 and 90 years, again consistent with a 65-year periodicity. It is the superposition of these two groups of cylinders (ML and EQ) that gives rise to the broad LOD maximum near 1900.

The correlation of individual cylinders with LOD (Fig. 6) indicates that angular momentum anomalies propagate from the equatorial to the polar cylinders. The total CAM (shown in red) results from the summation of the individual cylinders with a maximum at a 15-year lead with respect to LOD and secondaries at an 80-year lead and at a 60-year lag (note the -65-year periodicity). The color diagram vividly displays the ~65-year period with 4 maxima visible (two strong, two weak) and 4 minima. The strong

propagation pattern indicates that a period of ~ 60 years is required for a signal to be transmitted from the equatorial region to the polar cylinder. Similarly, a propagation pattern is evident in top line plots as the peaks and valleys are traced from one cylinder to another.

The torques responsible for angular momentum transfer between the Earth's atmosphere and the underlying planet are due to tractions produced by turbulent viscosity in the oceanic and continental boundary layers and also to topographic tractions due to normal pressure forces acting on orography. Topographic torques and boundary layer torques produced by atmospheric motions are typically comparable in magnitude but they have somewhat different temporal characteristics (5). Less is known about the torques at the Earth's core-mantle boundary (CMB), but it is generally considered that viscous effects are probably much less important than those due to Lorentz forces associated with electric currents in the lower reaches of the mantle, topographic torques associated with a bumpy core mantle boundary, and gravitational effects. Uncertainties about the electrical conductivity of the lower mantle and of the shape of the CMB and horizontal density variations in the mantle and core make it difficult at present to establish the relative importance of those agencies. One recent study (25) indicates that if topographic torques are of sufficient magnitude to explain the observed decadal LOD variations, and dominant contributions to the torque arise in the mid-latitude. This result could bear on our finding here that mid-latitude CAM fluctuations are in phase with fluctuations in the motion of the mantle. In addition, recent MHD results (12,13) showing robust activities at the mid-latitudes are consistent with this finding.

As to the roughly 65-year period seen in the angular momentum fluctuations presented in Figures 2 and 3, the simplest but by no means the only lines along which an interpretation might possibly be sought is to suppose that it can be identified with the main eigenmode of torsional MHD oscillations with $B_p \doteq 2 \times 10^{-4} \text{T}$ (see 26), where B_p is the average strength of the non-axial component of the poloidal magnetic field in the

core. This is about half the average strength of the (poloidal) magnetic field in the core mantle, which in turn is very much less than the likely strength ($\sim 10^{-2}$) of the toroidal component of the magnetic field within the Earth, which is effectively confined to the core (cf. equation (C4) of 26).

For the purpose of the present paper we note that torsional oscillations about the rotation axis (27) correspond to the case when $k = 0$ in Eq. C4. Then, Coriolis forces and Lorentz forces associated with the toroidal magnetic field are both negligible in comparison with Lorentz forces associated with the poloidal magnetic field, and Eq. (C4) reduces to $\omega^2 = V_p^2 / l^2$. The value of B_p is not known for the core; indeed the present work might provide the best estimate of B_p at present available! B_p could be as large as 10^{-3} T, but it might be much smaller if (as is possible but not certain) lines of force of the poloidal part of the geomagnetic field are aligned by core motions so that they are almost parallel to the Earth's rotation axis nearly everywhere within the core. Taking $B_p \doteq 4 \times 10^{-4}$ T we find $V_p \doteq 10^{-3}$ m s $^{-1}$, which is a factor of 25 smaller than $V_T \doteq 10^{-1}$ m s $^{-1}$ if (as is likely but not certain) $B_T \doteq 10^{-2}$ T (18). For length scales $2\pi l \doteq c$, the period of oscillation of the torsional mode c/V_p would be about 25 years (27, 28). This is less by a factor of about 20 than $\Omega c^2 / \pi^2 V_T^2$, the approximate period of any global-scale non-axisymmetric magnetostrophic oscillations as given by Eq. (C4) when, for example, $k = 1 \neq 0$ and $V_T / 2\Omega c \ll 1$ (18).

Such an eigenmode of MHD torsional oscillation would be readily excited by the fluctuating background of three-dimensional flow in the core if in the power spectrum of the fluctuation there is sufficient energy to overcome attenuation due (in this case) largely to ohmic dissipation associated with electric currents induced in the weakly-conducting lower mantle (29, 30). It is also possible of course that the 65-year period is not at all associated with MHD torsional oscillations in the core, and simply reflects the time scale of some dominant instability or nonlinear mode interaction responsible for angular momentum advection within the core. Beyond the scope of the present paper is any

detailed discussion of excitation and attenuation mechanisms and the role of advection and other nonlinear processes in the dynamics of torsional oscillations. The numerical models of core flow and the geodynamo that have been developed recently by various groups (see e.g. 12) could be used for such purposes in future research. Indeed, a stringent test of any such model would be its ability to simulate the geophysical phenomena revealed by this investigation of torsional oscillations of the Earth's core, which is based on observations of the geomagnetic field and of fluctuations in the Earth's rotation.

REFERENCES

1. J. A. Jacobs (ed.), *Geomagnetism* (4 vols), London: Academic Press (1987-1991).
2. R. Hide and J. O. Dickey, *Science* 253,629 (1991).
3. R. D. Rosen, *Surveys in Geophysics*, **14**, 1 (1993).
4. T. M. Eubanks, *Contributions of space geodesy to geodynamics* (ed. D. E. Smith and D. L. Turcotte)(Geodynamics Series Vol. 24, *Amer. Geophys. Un.*) p. 1 (1993).
5. R. M. Ponte, R. D. Rosen and G. J. Boer, *J. Climate*, 7,538 (1994).
6. J. O. Dickey, S. L. Marcus, and R. Hide, *Nature*, 357,484-488, 1992.
7. D. Jault and J.-L. Le Mou el, *Adv. Space Res.*, **13** (1 1) 221 (1993).
8. D. Jault, C. Gire and J.-L. Le Mou el, *Nature* 333,353 (1988).
9. X. Song and P. G. Richards, *Nature*, 382,221 (1996).
10. W.-J. Su, A. M. Dziewonski and R. Jeanloz, *Science*, 274, 1883 (1996).
11. J. M. Aurnou, D. Brito, and P. L. Olson, *Geophys. Res. Lett.*, 23,3401 (1996).
12. G. A. Glatzmaier and P. H. Roberts, *Nature*, 377, 203 (1995).
13. G. A. Glatzmaier and P. H. Roberts, *Science*, 274, 1887 (1996).
14. C. Jordi, L. V. Morrison, R. D. Rosen, D. A. Salstein, and G. Rossello, *Geophys. J. Intern.*, 117, 811-818 (1994).

15. F. R. Stephenson and L. V. Morrison. *Phil.Trans.Roy.Soc. A*, **351**, 165-202 (1995).
16. R. Hide, *Geophys.Res.Lett.*, 22, 961 (1995).
17. LeMouël, J-L., *Nature*, **311,734-735** (1984).
18. R. Hide, *Phil. Trans.Roy.Soc. A259*, 615 (1966).
19. R. Hide, Ph.D. Dissertation, Cambridge University (1953).
20. Co-axial cylindrical shells in the core.

To a first approximation, the liquid metallic outer core of the Earth occupies a region bounded by concentric spherical surfaces of radii b and c , where $b = 1222$ km and $c = 3480$ km. The volume and moment of inertia of the solid inner core are respectively much less than 10^{-1} and 10^{-2} times the volume and moment of inertia of the liquid outer core. An imaginary cylinder that is tangent to the inner sphere at the equator intersects the outer sphere at co-latitude $\theta = \theta^*$ in the northern hemisphere and $\pi - \theta^*$ in the southern hemisphere, where

$$\theta^* = \sin^{-1}(b/c). \quad (\text{A1})$$

The co-latitude angle θ^* is about 24° for the Earth (see *11,18,19*).

It is convenient to imagine the liquid core divided into an “extrapolar” liquid region E where $0^* < \theta < \pi - \theta^*$, and two “polar” liquid regions P where $0 < \theta < \theta^*$ in the Northern Hemisphere (NH) and $\pi - \theta^* < \theta < \pi$ in the Southern Hemisphere (SH). Consider a cylindrical shell in region E with bounding surfaces that intersect the outer spherical surface at co-latitudes θ_{q-1} and θ_q in the NH (and $\pi - \theta_{q-1}$ and $\pi - \theta_q$ in the SH) where $\theta^* \leq \theta_{q-1} < \theta_q \leq \pi/2$ (see Figure 1). The volume V_q of this cylindrical shell (in region E) is given by

$$V_q = \frac{4}{3} \pi c^3 [\cos^3 \theta_{q-1} - \cos^3 \theta_q] \quad (\text{A2})$$

(which follows from the so-called “apple core theorem” that the volume of a spherical apple that remains when an axisymmetric cylindrical core has been removed depends only on the length of the cut (31)). The corresponding combined volumes of the two identical cylindrical shells in polar regions P (where $0 < \theta < \theta^*$ and $\pi - \theta^* < \theta < \pi$) is given by

$$V_q = \frac{4}{3} \pi c^3 [\cos^3 \theta_{q-1} - \cos^3 \theta_q] - \frac{4}{3} \pi b^3 [\cos^3 \bar{\theta}_{q-1} - \cos^3 \bar{\theta}_q]. \quad (\text{A3})$$

Here $\bar{\theta}_{q-1}$ and $\bar{\theta}_q$ are the co-latitudes at which the inner and outer surfaces of the cylindrical shell intersects the surface of the inner sphere of radius b , so that

$$b \sin \bar{\theta}_q = c \sin \theta_q, \quad b \sin \bar{\theta}_{q-1} = c \sin \theta_{q-1}. \quad (\text{A4})$$

Equations (A1) to (A4) are expressions needed for the purpose of dividing up the liquid core into Q (say) imaginary co-axial cylindrical shells of equal volume. In the case of a full sphere ($b = 0$) (when the P regions shrink to zero volume), the volume of each cylindrical shell is equal to $4\pi c^3 / 3Q$, so that (by Eq. (A2)) we have

$$\theta_q = \cos^{-1} (1 - q/Q)^{1/3}, \quad (\text{AS})$$

where $q = 1, 2, \dots, Q$, and $\theta_Q = \pi/2$. The innermost shell, which has zero inner radius, extends from $\theta = 0$ to $\theta = \cos^{-1} (1 - Q^{-1})^{1/3}$. The outermost shell extends from $\theta = \pi/2$ to $\theta = \cos^{-1} Q^{-1/3}$. In the case when $b \neq 0$, it is necessary to use more complicated expressions based on equations (A3) and (A4) when calculating the latitudinal extent of the q th cylindrical shell. Values of θ_q in degrees are given in Table A1.

Table A 1

q	θ_q	q	θ_q	q	θ_q	q	θ_q
1	12.56	6	28.94	11	40.95	16	54.80
2	17.52	7	31.38	12	43.43	17	58.42
3	20.99	8	33.77	13	46.01	18	62.78
4	23.80	9	36.15	14	48.72	19	68.71
5	26.43	10	38.53	15	51.62	20	90.00

21. Determinations of core motions from geomagnetic secular variation data.

Denote by $\mathbf{B}(r, \theta, \phi, t)$ the value of the main geomagnetic field at the general point P with spherical polar coordinates (r, θ, ϕ) and by $\dot{\mathbf{B}} \equiv \partial \mathbf{B} / \partial t$ the GSV (I). Determinations of \mathbf{B} made at and near the Earth's surface at various epochs can be used to infer \mathbf{u}_s , the Eulerian flow velocity just below the core-mantle boundary (CMB) (see reference (32) for review). The first of the three geophysically-reasonable key assumptions that underlie the method used is that the electrical conductivity of the mantle and magnetic permeability gradients there are negligibly small, so that \mathbf{B} satisfies $\nabla \times \mathbf{B} = \mathbf{0}$ as well as $\nabla \cdot \mathbf{B} = 0$ and can therefore be expressed as the gradient of a potential U satisfying Laplace's equation $\nabla^2 U = 0$. This facilitates the downward extrapolation of the observed field at and near the Earth's surface in order to obtain \mathbf{B} and $\dot{\mathbf{B}}$ at the CMB.

The second assumption is that the electrical conductivity of the core is so high that when dealing with fluctuations in \mathbf{B} on time scales that are very much less than that of the ohmic decay of magnetic fields in the core (which is several thousand years for global-scale features) \mathbf{B} satisfies Alfvén's "frozen flux" theorem expressed by the equation

$$\partial \mathbf{B} / \partial t = \nabla \times (\mathbf{u} \times \mathbf{B}). \quad (\text{B1})$$

To this approximation, the lines of magnetic force emerging from the core are advected by the horizontal flow (v_s, w_s) just below the CMB. Accordingly, if $\mathbf{B} = (B_r, B_\theta, B_\phi)$, the radial component B_r at the CMB satisfies

$$\frac{\partial B_r}{\partial t} + \frac{v_s}{c} \frac{\partial B_r}{\partial \theta} + \frac{w_s}{c \sin \theta} \frac{\partial B_r}{\partial \phi} = B_r \left[\frac{\partial u}{\partial r} \right]_{r=c} \quad (132)$$

(.23, 34).

A third assumption is needed to secure uniqueness, and one physically-plausible possibility is that to a first approximation the flow in the upper reaches of the core—the “polosphere” (16)—is in geostrophic balance with the pressure field there (17, 32, 35), which can be shown to imply that

$$\frac{\partial}{\partial \theta} (v_s \sin \theta \cos \theta) + \cos \theta \frac{\partial w_s}{\partial \phi} = 0 \quad (B3)$$

in the case of an incompressible fluid, for which $\nabla \cdot \mathbf{u} = 0$

Various groups of geomagnetic workers have produced maps of $\mathbf{u}_s = (v_s, w_s)$ and investigated the errors and uncertainties encountered in practice (32, 35). These hypothetical flow fields \mathbf{u}_s are all similar in their general appearance but there are discrepancies between them which remain to be resolved by future research. Most determinations of \mathbf{u}_s from GSV data make use of spherical harmonic expansions of the variables involved. Here we follow the treatment of reference (32) where the starting point for the spectral expansion of \mathbf{u} is its separation into toroidal and poloidal components. Thus

$$\mathbf{u} \equiv \mathbf{u}_T + \mathbf{u}_P \equiv \nabla \times (T\mathbf{r}) + \nabla_1(rS) \quad (B4)$$

(where ∇_I is the “horizontal” gradient operator), so that

$$\mathbf{u}_T = \left[0, \frac{1}{\sin \theta} \frac{\partial T}{\partial \phi}, \frac{\partial T}{\partial \theta} \right]. \quad (\text{B5})$$

$$\mathbf{u}_S = \left(0, \frac{\partial S}{\partial \theta}, \frac{1}{\sin \theta} \frac{\partial S}{\partial \phi} \right). \quad (\text{B6})$$

The potentials T and S are expanded in spherical harmonics

$$T(\theta, \phi) = \sum_{l,m} t_l^m Y_l^m(\theta, \phi) \quad (\text{B7})$$

$$S(\theta, \phi) = \sum_{l,m} s_l^m Y_l^m(\theta, \phi) \quad (\text{B8})$$

where the Y_l^m are real Schmidt quasi-normalized spherical harmonics. Thus, we can write

$$\mathbf{u}_T = \sum_{l,m} t_l^m \mathbf{T}_l^m, \quad \mathbf{u}_S = \sum_{l,m} s_l^m \mathbf{S}_l^m \quad (\text{B9a, b})$$

where

$$\mathbf{T}_l^m = \nabla \times (Y_l^m \mathbf{r}), \quad \mathbf{S}_l^m = r \nabla_{\perp} Y_l^m \quad (\text{B10a,b})$$

It follows from these expressions that the azimuthal component $w_{,\phi}$ (6,+ , t) of \mathbf{u} , satisfies:

$$w_{,\phi}(\theta, \phi, t) = \sum_{l,m} \left[-t_l^m \frac{\partial Y_l^m}{\partial \theta}(\theta, \phi) + s_l^m \frac{\partial Y_l^m}{\sin \theta \partial \theta}(\theta, \phi) \right]. \quad (\text{B11})$$

from which we are able to evaluate $\mu_q(t; Q)$ (see (Eq. 3)). When combined with Eq. (S) and (6), this gives for $M(t)$ the equation

$$M(t) = 2\pi\bar{\rho}_c^4 \left[\frac{4}{15} t_1^0 + \frac{16}{35} t_3^0 \right] \quad (\text{B } 12)$$

in the absence of a solid inner core (i.e., when $b = 0$), in agreement with an expression for $M(r)$ given in references (32) and (35).

22. D. Jault and J.-L. Le Mouél, *J. Geomag. Geoelect.* 43, 111 (1991).

23. A. Jackson, J. Bloxham and D. Gubbins, in *Dynamics of Earth's deep interior and Earth rotation* (ed. J.-L. Le Mouél, D. E. Smylie and T. A. Herring), *Geophys. Monog. Amer. Geophys. Un.* 72,97 (1993).

24. S. R. C. Malin and B. M. Hodder, *Nature*, 296, 726-728 (1982).

25. R. Hide, R. W. Clayton, B. H. Hager, M. A. Spieth and C. V. Voorhies, in *Relating geophysical structures and processes: The Jeffreys Volume* (ed. K. Aki and R. Dmowska), *Geophys. Monog. Amer. Geophys. Un.*, 76, 107-120(1993).

26. Magnetohydrodynamic oscillations of a rotating fluid.

General theoretical considerations indicate that the Earth's liquid outer core can in principle support a wide range of transverse ("shear") oscillations at subseismic frequencies, with periods ranging from less than a day to centuries. The restoring forces involved are (a) gyroscopic (Coriolis) forces associated with the Earth's rotation, (b) ponderomotive (Lorentz) forces associated with the geomagnetic field, and (c) buoyancy (Archimedes) forces due to the action of gravity on density inhomogeneities in any bottom-heavy regions, where the potential density decreases upward. Generated by internal instabilities and/or external forcing, the oscillations would be modified by background flows and nonlinear interactions of various kinds.

Coriolis forces render core motions highly anisotropic, with certain properties that are roughly independent of direction parallel to the rotation axis. One particularly important class of slow *non-axisymmetric* oscillations, characterized by near “magnetostrophic balance” between Coriolis and Lorentz restoring forces associated largely with the *toroidal* part of the geomagnetic field, is probably manifested in the main features of the geomagnetic secular variation (GSV) on time scales of centuries (18, 36). The restoring forces associated with any *axisymmetric* torsional oscillations about the rotation axis would be provided solely by Lorentz forces associated with azimuthal displacements of the *poloidal* part of the geomagnetic field (27, 28), giving much shorter oscillation periods, namely decades rather than centuries.

Insight into oscillations of a continuous medium can be obtained by first considering the simplest-imaginable elementary small-amplitude plane waves in a medium of infinite extent with uniform background properties when dissipative effects can be neglected. For oscillations of the Earth’s core at subseismic frequencies (i.e. with periods greater than about an hour), these are disturbances of the form $\cos(\omega t - \boldsymbol{\kappa} \cdot \mathbf{r})$ of an effectively incompressible inviscid liquid of zero electrical resistivity immersed in a steady and uniform magnetic field \mathbf{B}_0 when the whole system rotates with steady angular velocity $\boldsymbol{\Omega}$ relative to an inertial frame. Here t denotes time, ω the angular frequency of the oscillation, \mathbf{r} is the vector position of a general point P in the rotating frame with Cartesian coordinates (x, y, z) , and $\boldsymbol{\kappa} = (k, l, m)$ is the vector wave number of the oscillation. The phase and group velocities of the wave are $(\omega/k, \omega/l, \omega/m)$ and $(\partial\omega/\partial k, \partial\omega/\partial l, \partial\omega/\partial m)$ respectively.

Denote by μ the constant magnetic permeability of the liquid, by $\bar{\rho}$ its mean density, and by

$$V \equiv B_0 / (\mu \bar{\rho})^{1/2} \quad (c1)$$

the constant so-called “Alfvén” velocity, a quantity of fundamental importance in MI ID. Denote by \mathbf{g} the background gravitational field (including centripetal effects) and suppose for simplicity that the vector

$$N \equiv (\mathbf{g} \cdot \nabla \rho_o / \bar{\rho})^{1/2} \mathbf{g} / |\mathbf{g}| \quad (\text{C2})$$

is constant, where the background density is $\bar{\rho} + \rho_o(\mathbf{r})$ with $\mathbf{g} \times \nabla \rho_o = \mathbf{0}$. The magnitude of N is the so-called Brunt-Väisälä frequency, which is real when the system is bottom heavy (i.e., $\mathbf{g} \cdot \nabla \rho_o > 0$), zero in the neutral case when ($\mathbf{g} \cdot \nabla \rho_o = 0$), and imaginary in the unstable situation when the system is top-heavy (i.e. $\mathbf{g} \cdot \nabla \rho_o < 0$). The assumption of incompressibility effectively filters out longitudinal (compressional) waves, leaving only transverse (shear) waves in which particle displacements have no component parallel to the wave fronts. The dispersion relationship between ω and κ is given by:

$$\omega^4 - \omega^2 (2\omega_V^2 + \omega_N^2 + \omega_\Omega^2) + \omega_V^2 (\omega_V^2 + \omega_\Omega^2) = 0 \quad (\text{C3})$$

(37), where $\omega_V^2 \equiv (\mathbf{V} \cdot \boldsymbol{\kappa})^2$, $(L) := (\mathbf{N} \times \boldsymbol{\kappa})^2 / \kappa^2$ and $\omega_\Omega^2 \equiv (2 \boldsymbol{\Omega} \cdot \boldsymbol{\kappa})^2 / \kappa^2$, which gives $\omega = 0$ (i.e., no transverse waves) when $\omega_V = \omega_N = \omega_\Omega = 0$.

Geophysical fluid dynamicists are concerned with a rich variety of waves corresponding to various limiting cases of Eq. (C3). Thus, when $2\boldsymbol{\Omega} \neq \mathbf{0}$ but $\mathbf{N} = \mathbf{V} = \mathbf{0}$ we have the elementary pure “(elastoid) inertial” waves (38); when $\mathbf{N} \neq \mathbf{0}$ but $\mathbf{V} = 2\boldsymbol{\Omega} = \mathbf{0}$, we have “internal (gravity)” waves (39); and when $\mathbf{V} \neq \mathbf{0}$ but $2\boldsymbol{\Omega} = \mathbf{N} = \mathbf{0}$, we have the “MHD (Alfvén)” waves (40). Certain classes of hybrid waves arise not only when $2\boldsymbol{\Omega} \neq \mathbf{0}$, $\mathbf{N} \neq \mathbf{0}$, $\mathbf{V} \neq \mathbf{0}$ (37), but also when $2\boldsymbol{\Omega} \neq \mathbf{0}$ and $\mathbf{N} \neq \mathbf{0}$ but $\mathbf{V} = \mathbf{0}$, the case of “inertia-gravity” waves (38); when $\mathbf{h}' \neq \mathbf{0}$ and $\mathbf{V} \neq \mathbf{0}$ but $2\boldsymbol{\Omega} = \mathbf{0}$, the case of “MH-gravity” waves; and when $\mathbf{V} \neq \mathbf{0}$ and $2\boldsymbol{\Omega} \neq \mathbf{0}$ but $\mathbf{N} = \mathbf{0}$, the case of “MHD-inertial” waves (41). And in the case of a semi-infinite rather than an infinite medium many types of edge waves are also possible, for imaginary components of κ normal to the boundary of the

medium then become admissible. These edge waves include the well-known Kelvin waves (19) which, with the related inertia-gravity waves, are important in dynamical oceanography and meteorology. as well as certain MHD edge waves (42) that are possible in rotating stratified fluids when $\mathbf{V} \neq 0$, $2\Omega \neq 0$ and $N \neq 0$.

Further insight into the processes involved is derivable from studies of the dispersion relationships and other properties of plane waves, such as particle trajectories, polarization, etc., but complications arise when dealing with actual geophysical systems. The finite dimensions of the fluid medium have to be taken into account in cases when they cannot be treated as large in comparison with the scales of the eigenmodes of oscillation. Thus, related to the ‘‘MHD-inertial’’ plane waves whose dispersion relationship is given by Eq. (3) with $N = 0$ are the so-called ‘‘MHD-planetary’’ waves (18, 43, 44, 45) with properties affected by the presence of (nearly) spherical boundaries, as in the case of the Earth’s core. An approximate dispersion relationship for such waves is given by

$$\omega^2 + \alpha k \omega / (k^2 + l^2) - (V_T k + V_P l)^2 = 0 \quad (C4)$$

(18), where $V_T \equiv B_T / (\mu \bar{\rho})^{1/2}$ and $V_P \equiv B_P / (\mu \bar{\rho})^{1/2}$ if B_T is a measure of the strength of the azimuthal (toroidal) magnetic field in the core and B_P that of the strength of the non-axial component of the meridional (poloidal) field, and k and l are the east-west and south-north wave numbers. For disturbances that are largely confined to the ‘‘polar’’ regions (see Figure 1) where the latitude exceeds 66° (at which the cylinder tangent at the equator to the outer boundary of the solid inner core meets the outer boundary of the liquid core), the quantity $\alpha \doteq 2\Omega/c$ where c is the outer radius of the liquid core and Ω is the basic angular speed of rotation of the system. On the other hand, for disturbances that are largely confined to the ‘‘extrapolar’’ regions which occupy more than 90% of the whole core, the quantity $a \doteq -\Omega/c$ (4).

27. S. I. Braginsky, *Geomag. Aeron.* **10**, 3 (1970).
28. S. I. Braginsky, *Geophys. Astrophys. Fluid Dyn.* 30, 1 (1984).
29. R. Hide and P. H. Roberts, *Advances in Applied Mechanics*, 4, 215 (1962).
30. P. H. Roberts, *J. Geomag. Geoelect.*, **24**, 231 (1972).
31. R. Hide and I. N. James, *Geophys. J. Roy. Astron. Sm.*, 74, **301 (1983)**.
32. J. Bloxham and A. Jackson, *Rev. Geophys.* 29,97 (1991).
33. P. H. Roberts and S. Scott, *J. Geomag. Geoelect.*, 17, 137 (1965).
34. G. E. Backus, *Phil. Trans. Roy. Soc. A26*, 3,239 (1968).
35. C. Gire and J.-L. Le Mouél, *Phys. Earth Planet. Inter.* 59,259 (1990).
36. S. I. Braginsky, *Geomag. Aeron.* **7**, 1050(1967).
37. R. Hide, *J. Fluid Mech.* 39,283 (1969).
38. H. P. Greenspan, *The theory of rotating fluids*, Cambridge University Press (1968).
39. A. E. Gill, *Atmosphere-ocean dynamics*, New York: Academic Press (1982).
40. T. G. Cowling, *Magnetohydrodynamics*, Bristol: Adam Hilger (1976).
41. B. Lehnert, *Astrophys. J.*, **119**,647 (1954).
42. D. G. Andrews and R. Hide, *J. Fluid Mech.* 72, 593 (1975).
43. W. V. R. Malkus, *J. Fluid Mech.*, 28,793 (1967).
44. R. Hide and K. Stewartson, *Rev. Geophys. Space Phys.* **10**,579 (1972).
45. D. J. Acheson and R. Hide, *Rept. Prog. Phys.* 36, 159 (1973).
46. We are greatly indebted to Dr. Andrew Jackson for providing the velocity data used in our investigation. We also acknowledge helpful discussions with David Barraclough, Danan Dong, and Richard S. Gross and Steven L. Marcus for helpful comments. The work of the authors presents the results of one phase of research carried out at the Jet Propulsion Laboratory, California Institute of Technology, sponsored by the National Aeronautics and Space Administration.

Legends for Diagrams and Tables

Figure 1. Illustrating the division of the Earth's liquid outer core into $Q = 20$ annular regions of equal volume numbered $q = 0, 1, 2, 3 \dots 20$ and bounded on the equatorward side by the co-latitude θ_q in the Northern Hemisphere and $\pi - \theta_q$ in the Southern Hemisphere, where values of θ_q are shown in Table A 1, see (20).

Figure 2. (a) Temporal fluctuations in $\mu_q(t; Q)$, $q = 0, 1, 2, 3 \dots Q = 20$, the angular momentum of each annulus, from 1840 to 1990 (thin lines) and of $M(t)$, the total angular momentum (thick line) (see Eq. 5 and 6 and Figure 2(b)); (b) The dependence on q of the temporal mean value of $\mu_q(t; Q)$, the core angular momentum, from 1840 to 1980 (thick broken line) and of the range of temporal fluctuations (thin broken lines).

Figure 3. Three-dimensional representation of core angular momentum of 20 co-axial equi-volume cylindrical shells as a function of cylinder number and time (Hovmöller diagram). Note the dominant -65-year fluctuation and its latitude dependence.

Figure 4. Comparison of length of day (LOD) and core angular momentum (CAM). A slope of 1.7 ms/century has been removed from the LOD data to allow for the effects of post-glacial rebound and the secular acceleration of the moon and a 10-year smoothed series are shown from each of the series. The total CAM (M) is shown as well as three regions (cylinders 1-3, 4-15, 16-20). Note the large correlation between LOD and midlatitude region (belts 4-15).

Figure 5. The correlation of grouped cylinders (1-3, 4-15, 16-20) of CAM with LOD as a function of lag of the CAM with respect to the LOD. The top curve (a) is based on the

full series (1840-1990), and (he bottom curve (b) on the shorter series (1867.5-1990) where the correlation is higher.

Figure 6. Correlation of LOD (length of day) with the CAM (core angular momentum) as a function of the lag of the CAM with respect to the length of day. The effect of the individual bands are shown in black and by the color graphics; the total CAM effect is depicted by the red line.

Table 1. Statistical data relating to Figure 3.

Table A1. Values of θ_m , in degrees, where $m = 0, 1, 2, 3, \dots, n (= 20)$, based on equations (A3)–(A5) (see 20).

CAM _i /CAM _{TOTAL}					CAM _i /LOD			
Belts	Correlation Lag = 0	Max Correlation	Lag (years) at max Correlation	% Variance Explained	Correlation Lag = 0	Maximum Correlation	Lag (years) at max Correlation	% variance Explained
1	.16	.33	15	.2	.20	.22	-2.5	.4
2	.32	.48	12.5	1.6	.32	.36	-2.5	2.5
3	.48	.61	7.5	2.8	.42	.44	-2.5	3.9
4	.62	.74	7.5	3.8	.50	.52	-2.5	5.0
5	.73	.83	7.5	4.8	.55	.58	-2.5	5.8
6	.79	.86	5	5.6	.56	.58	-2.5	6.4
7	.81	.86	5	6.3	.54	.56	-2.5	6.7
8	.81	.83	2.5	6.7	.51	.53	-2.5	6.8
9	.80	.81	2.5	7.0	.47	.49	-2.5	6.6
10	.79	.79	2.5	7.0	.42	.45	-2.5	6.0
11	.78	.78	0	6.8	.38	.41	-5	5.2
12	.79	.79	0	6.4	.32	.40	-10	4.2
13	.81	.81	0	5.9	.25	.41	-12.5	2.9
14	.84	.84	0	5.2	.16	.48	-20	1.4
15	.81	.81	0	4.4	-.02	.61	-20	-.2
16	.66	.66	0	3.7	-.21	.67	-22.5	-1.9
17	.46	.56	-15	3.2	-.33	.66	-25	-3.6
18	.36	.58	-15	3.2	-.37	.65	-25	-5.2
19	.39	.62	-15	4.3	-.36	.67	-25	-6.3
20	.59	.69	-7.5	11.28	-.17	.64	-22.5	-5.4
1-3	.38	.53	10	4.6	.36	.38	-2.5	6.9
4-15	.88	.88	2.5	69.8	.47	.49	-7.5	56.9
16-20	.56	.69	-7.5	25.6	-.31	.74	-25	-22.5
Total 1-20	1.0	1.0	0	100	.26	.58	-17.5	41.3

Full CAM Series

CAM _i /CAM _{TOTAL}					CAM _i /LOD			
Belts	Correlation Lag = 0	Max Correlation	Lag (years) at max Correlation	% Variance Explained	Correlation Lag = 0	Maximum Correlation	Lag (years) at max Correlation	% variance Explained
1	.46	.74	17.5	.8	.27	.35	-7.5	.6
2	.57	.80	15	3.9	.40	.43	-2.5	3.2
3	.65	.84	12.5	5.3	.51	.52	-2.5	5.0
4	.71	.87	7.5	6.1	.61	.61	0.0	6.3
5	.75	.89	7.5	6.5	.69	.69	0.0	7.2
6	.75	.86	7.5	6.6	.75	.75	0.0	7.9
7	.72	.79	5	6.5	.77	.77	0.0	8.3
8	.68	.72	5	6.2	.77	.77	0.0	8.4
9	.63	.65	2.5	5.7	.75	.75	0.0	8.2
10	.58	.59	2.5	5.2	.72	.72	0.0	7.6
11	.55	.55	0.0	4.5	.70	.70	0.0	6.8
12	.55	.55	0.0	3.9	.68	.68	0.0	5.7
13	.58	.58	0.0	3.2	.66	.66	0.0	4.4
14	.64	.64	0.0	2.7	.57	.58	-2.5	2.9
15	.57	.57	0.0	2.3	.25	.52	-10.	1.2
16	.38	.54	-15.	2.2	-.08	.51	-20.	-.6
17	.30	.59	-15.	2.7	-.22	.56	-20.	-2.3
18	.33	.65	-15.	3.9	-.27	.61	-22.5	-3.8
19	.43	.75	-15.	6.6	-.27	.67	-22.5	-4.9
20	.58	.76	-7.5	15.2	-.12	.57	-22.5	-3.7
1-3	.60	.81	15	10.0	.44	.46	-2.5	8.8
4-15	.76	.78	2.5	59.4	.80	.80	0.0	74.9
16-20	.51	.77	-15	30.6	-.21	.67	-22.5	-15.3
Total 1-20	1.0	1.0	0.	100	.57	.64	-5	68.4

Shorter CAM Series

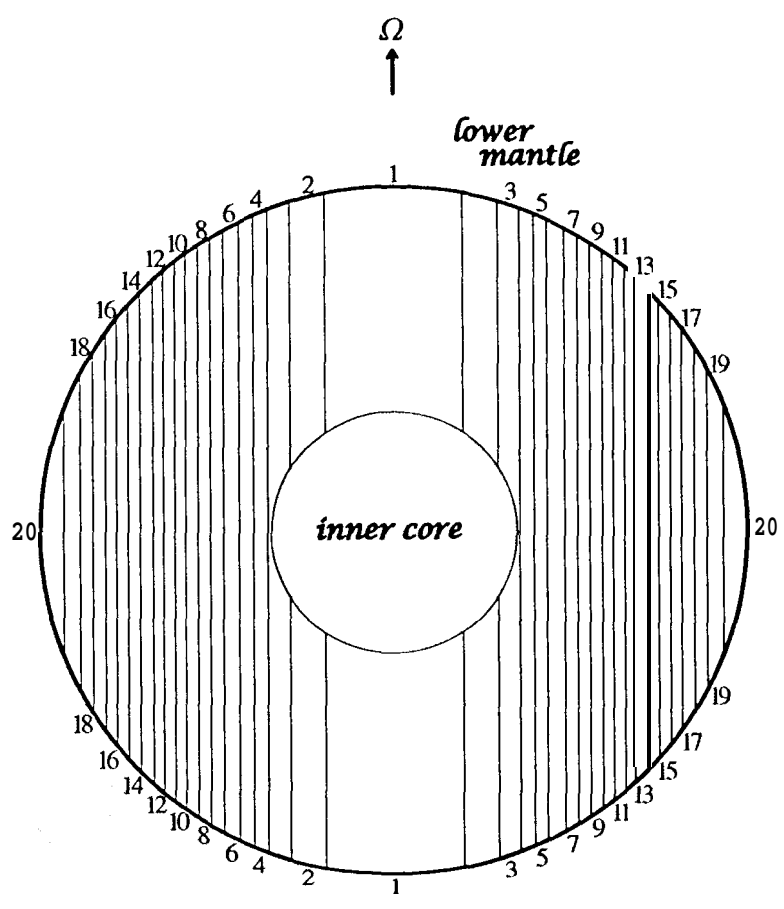


Figure 1

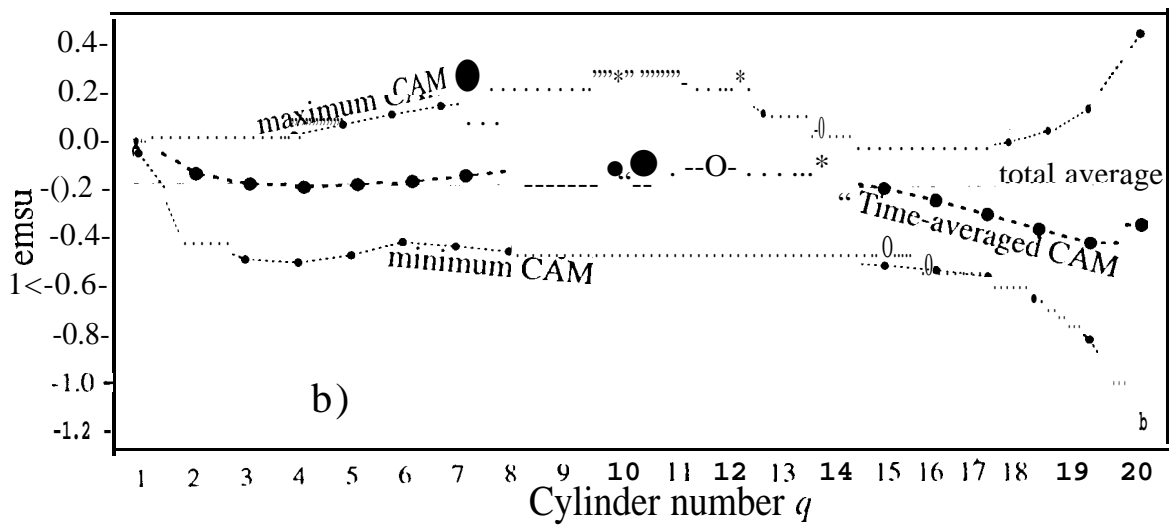
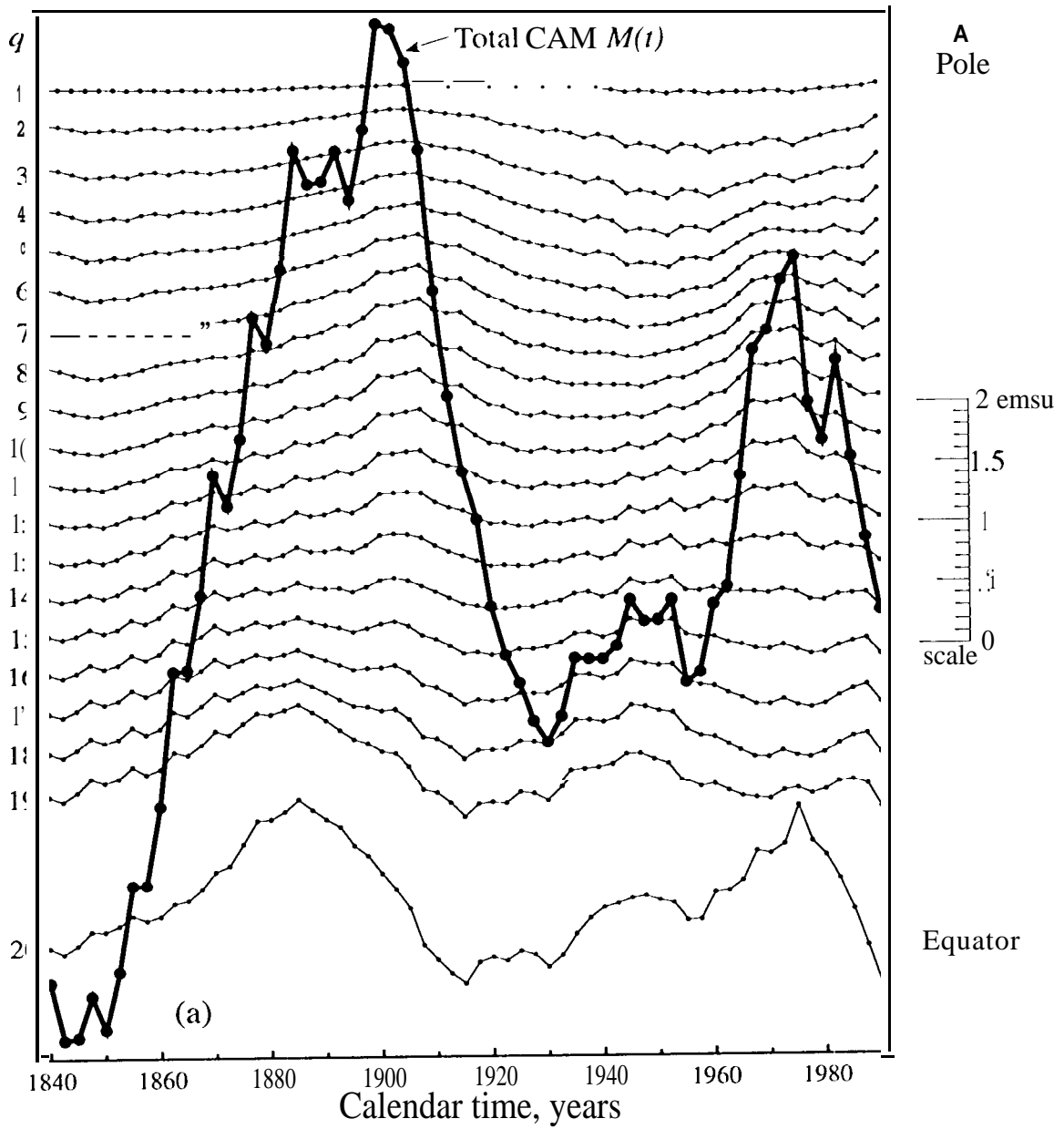


Figure 2

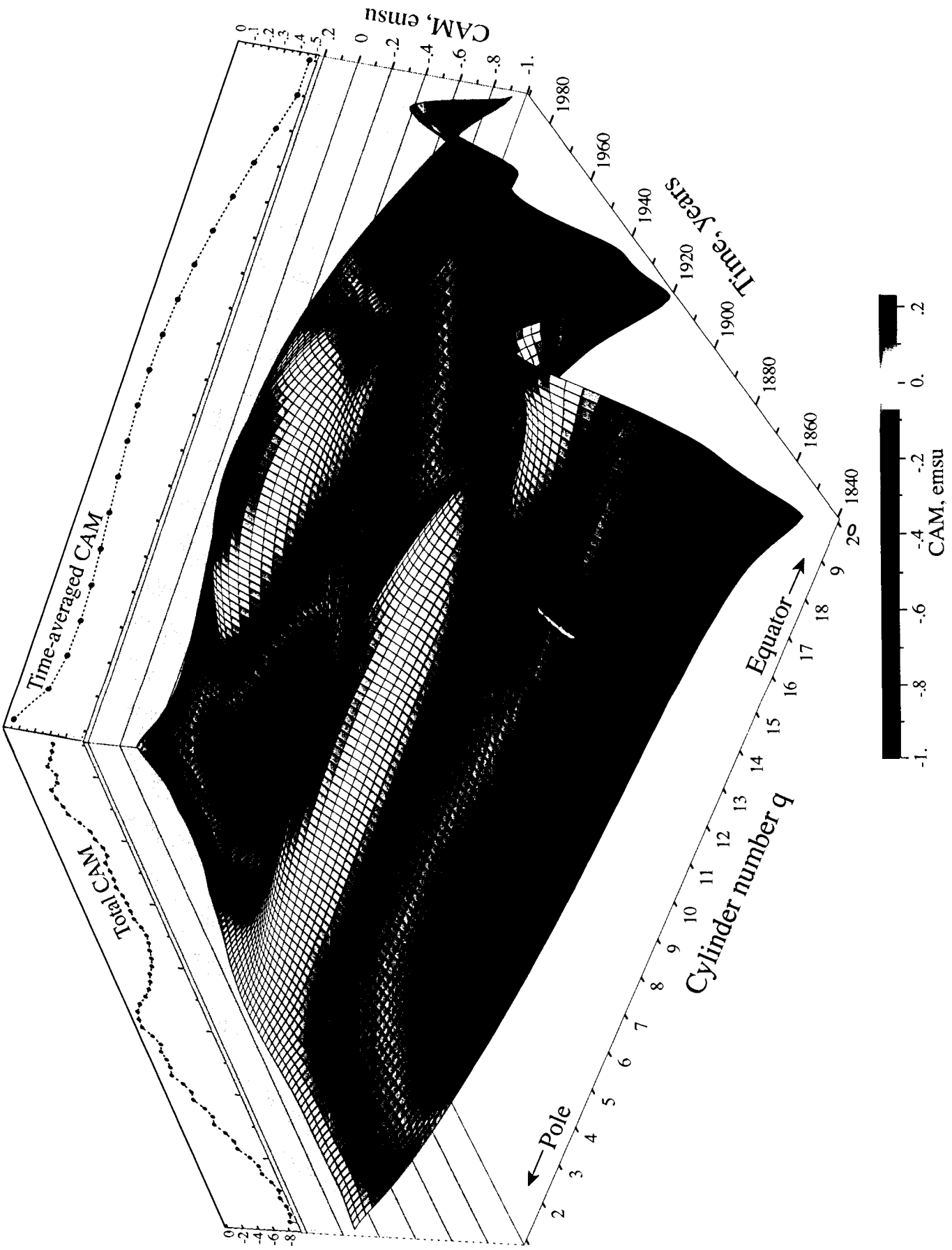


Figure 3(a)

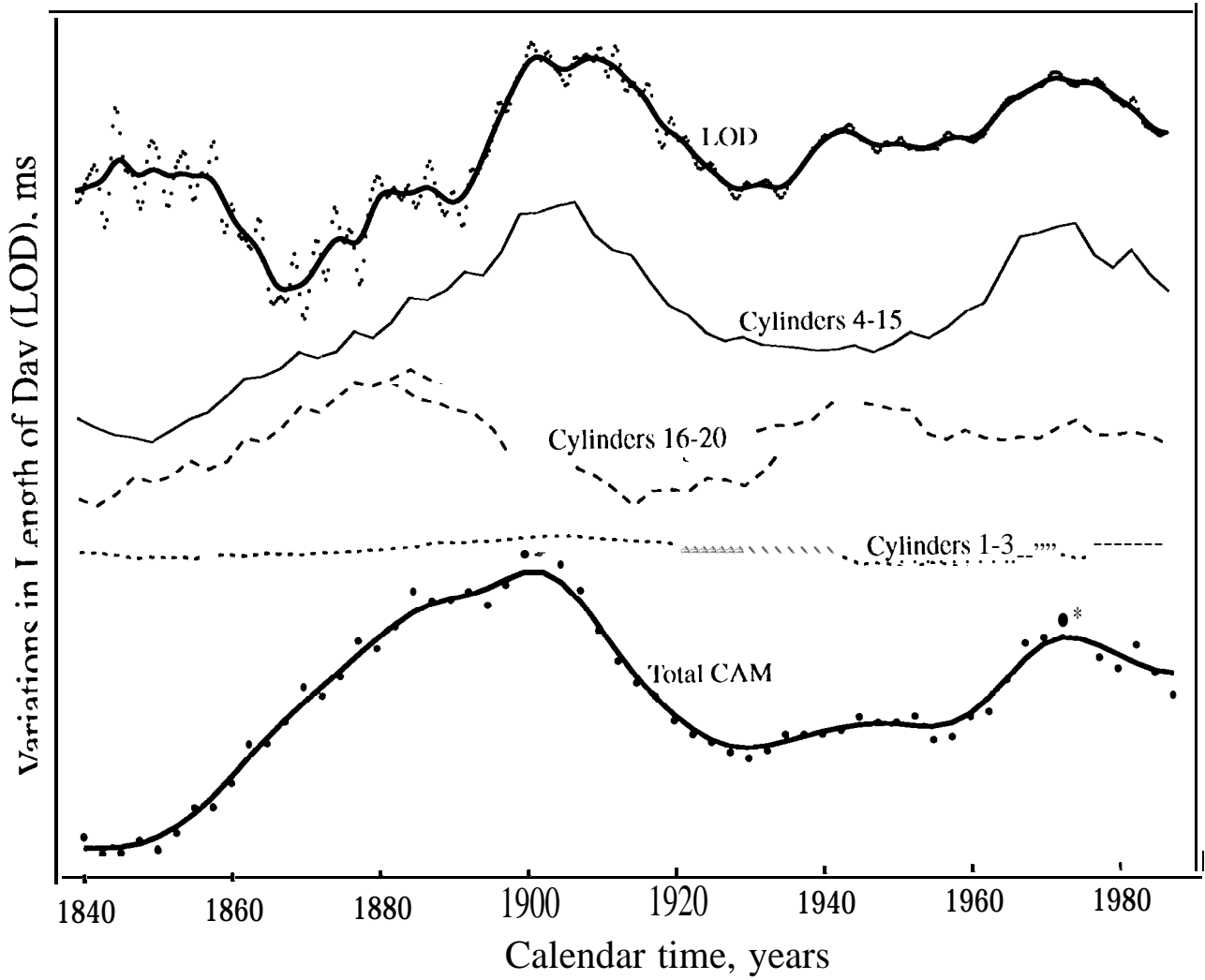


Figure 4

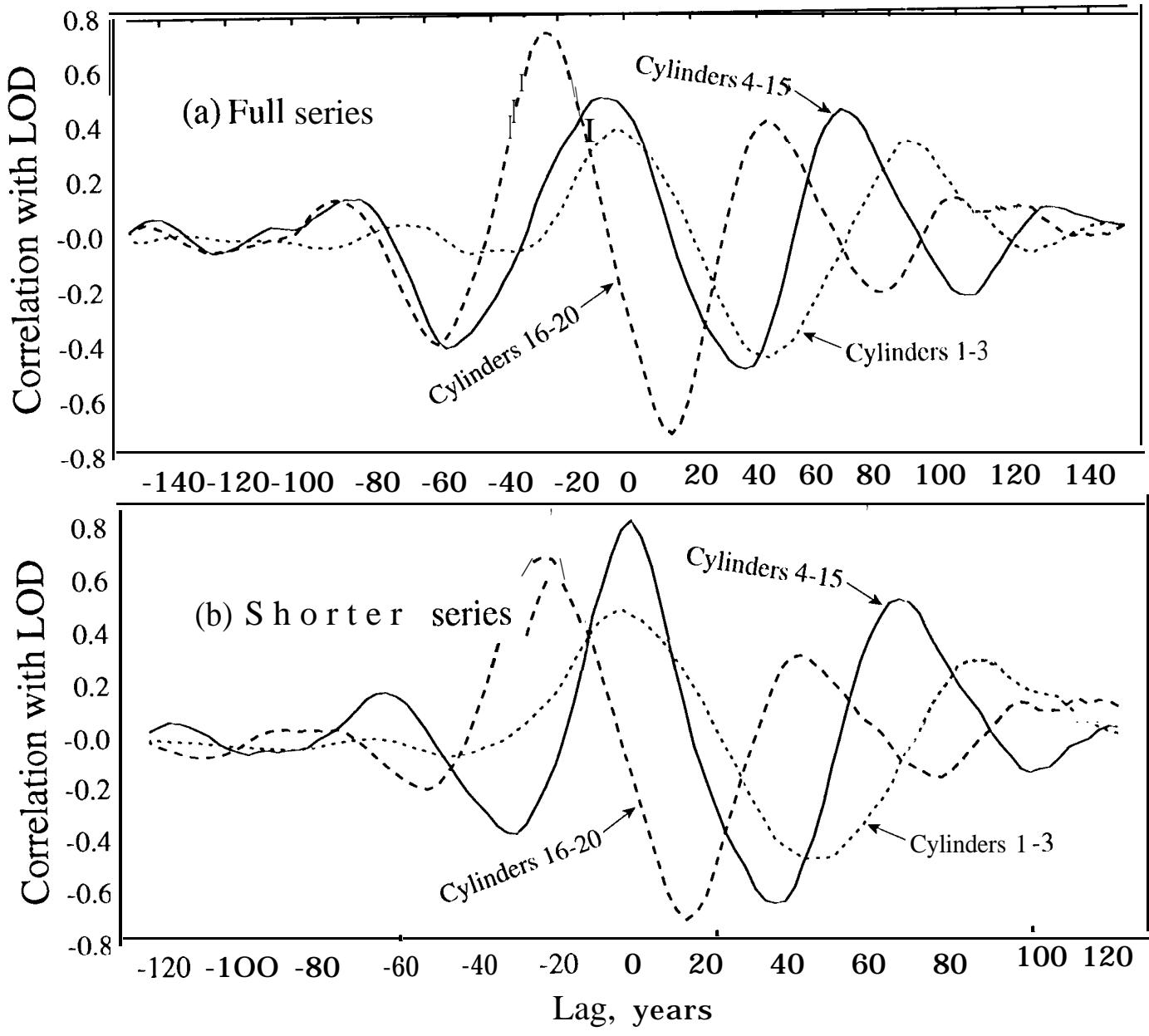


Figure 5

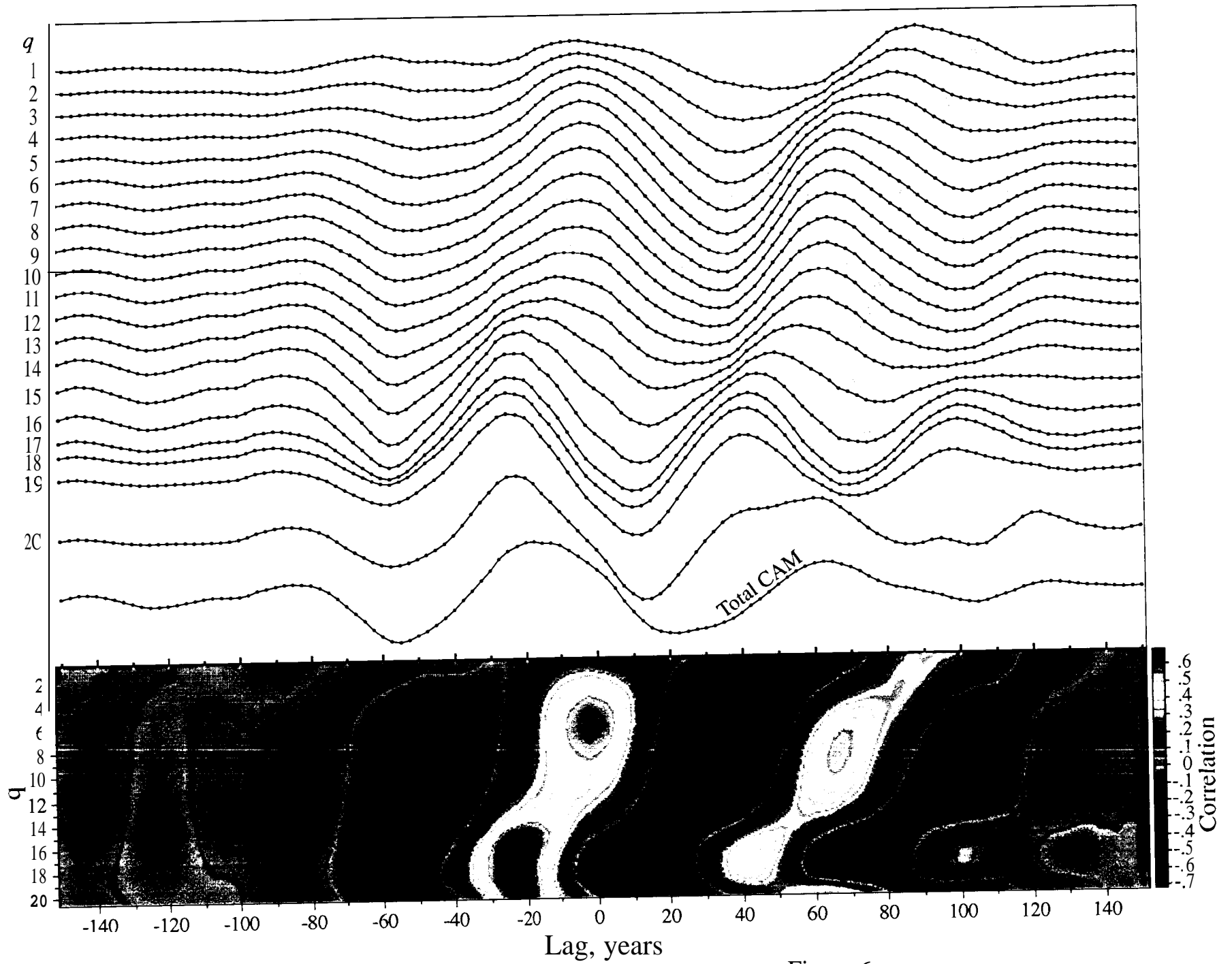


Figure 6